Supplement of Atmos. Chem. Phys., 25, 14501–14511, 2025 https://doi.org/10.5194/acp-25-14501-2025-supplement © Author(s) 2025. CC BY 4.0 License.





Supplement of

Heterogeneous impacts of fire-sourced ozone (O_3) pollution on global crop yields in the future climate scenarios

Rui Li et al.

Correspondence to: Dongmei Tang (dmtang@geo.ecnu.edu.cn) and Hongfang Zhao (hfzhao@geo.ecnu.edu.cn)

The copyright of individual parts of the supplement might differ from the article licence.

Three statistical indicators including determination coefficient (R²), root mean square error (RMSE), and mean absolute error (MAE) were applied to validate the modelling performances of ambient MDA8 O₃ concentration (Li et al., 2019; Li et al., 2023). P_i and O_i represent the predicted and observed concentrations, respectively. SSR and SST represent the regression sum of squares and total sum of squares, respectively. The detailed equations are as follows:

$$R^{2} = \frac{SSR}{SST} \quad (S1)$$

$$RMSE = \sqrt{\frac{\sum_{i=1}^{N} (P_{i} - O_{i})^{2}}{N}} \quad (S2)$$

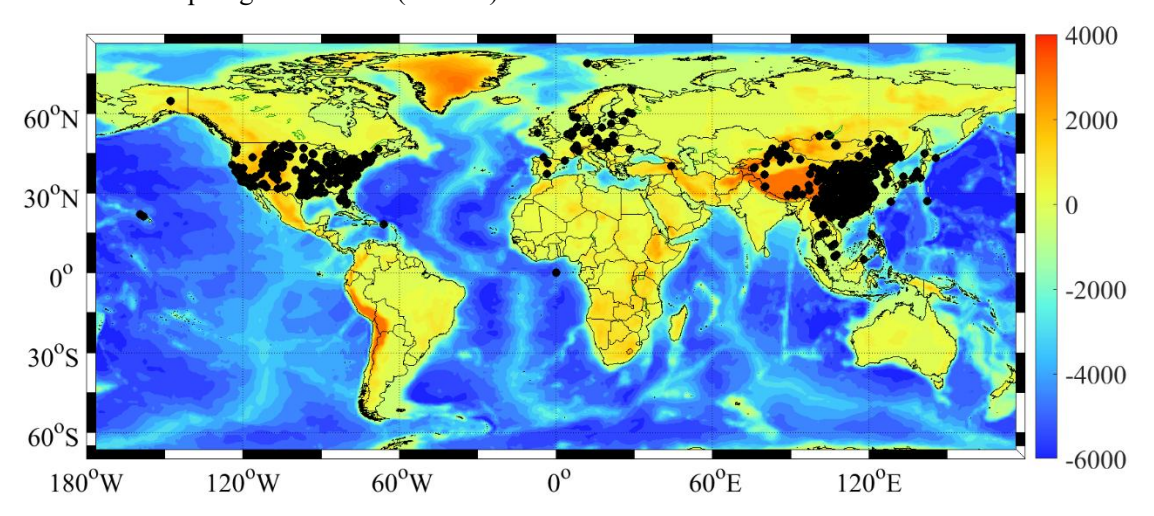
$$MAE = \sum_{i=1}^{N} |P_{i} - O_{i}| \quad (S3)$$

Besides, some redundant variables were also removed in the final model because it might degrade the predictive accuracy of the multi-stage model.

Table S1 The updated AOT40 response function for major four crops.

	Equation	References
Maize	RY=-0.0058AOT40+1	1
Rice	RY=-0.009489AOT40+1	2
Spring wheat	RY=-0.0205AOT40+1	3
Winter wheat	RY=-0.0205AOT40+1	3

Figure S1 The ground-level observations of O_3 concentrations at the global scale. The color bar reflects the map of global terrain (altitude).



Step1 **MERRA2** reanalysis **GEOS-Chem** GCAP reanalysis ozone wildfire **GEOS-Chem** Historical anthropogenic (v13.4.0)emission **GEOS-Chem** SSP scenario emission ozone total Step2 Meteorological Satellite products data Global optimized **XGBoost** Population total ozone in Land use data data model 2010s, 2040s, and 2090s CMIP6 Observation total ozone ozone Step3 Global distribution pattern of wildfire-induced ozone Global optimized 60°N 30°N wildfire-induced 0^{o} ozone during 2040s 30°S 60°S and 2090s 180°W 120°W 60°W 60°E 120°E Impact of future wildfire emission on ambient O3 exposure and crop yield

Figure S2 The workflow of wildfire-induced O₃ concentration and crop yield loss estimates.

Figure S3 The predictive accuracy of MDA8 O_3 concentrations at the global scale (a). The relationship between fire-sourced MDA8 O_3 level and K^+ concentration (b). The relationship between fire-sourced MDA8 O_3 level and levoglucosan concentration (c).

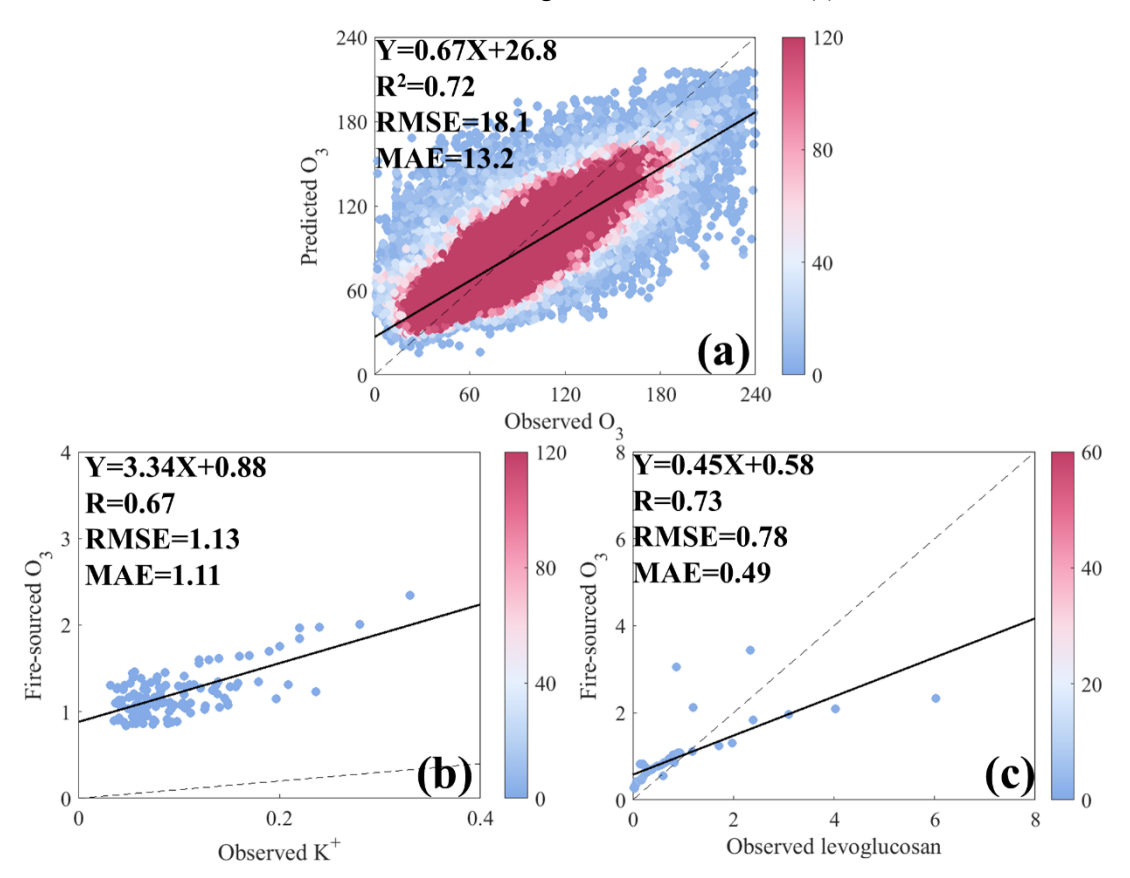


Figure S4 The global variations of wildfire-induced 8-h O_3 levels (Unit: $\mu g/m^3$) in SSP1-2.6 (a), SSP3-7.0 (b), and SSP5-8.5 (c) scenarios during 2090s. The spatial distributions of wildfire-related 8-h O_3 concentrations (Unit: $\mu g/m^3$) in different regions during 2090s (d). US, SA, and SS represent the United States, South America, and Sub-Sahara Africa, respectively.

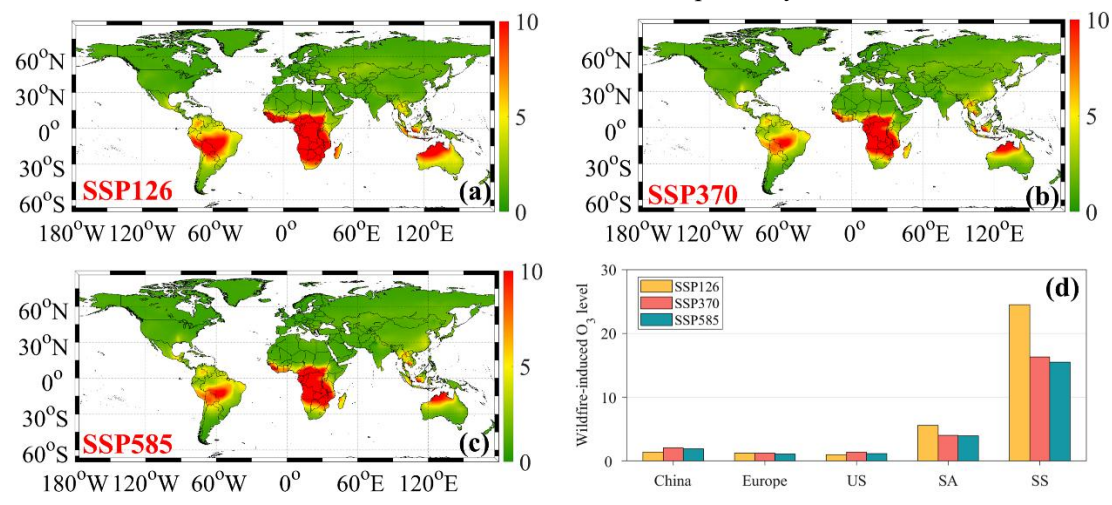


Figure S5 The global variations of wildfire-induced O₃-related rice yield losses (Unit: t/km²) during historical (a), SSP1-2.6 (b), SSP3-7.0 (d), and SSP5-8.5 (e) scenarios during 2040s, respectively. The spatial variations of wildfire-induced rice yield losses (Unit: t/km²) in major regions during 2040s. US, SA, and SS represent the United States, South America, and Sub-Sahara Africa, respectively.

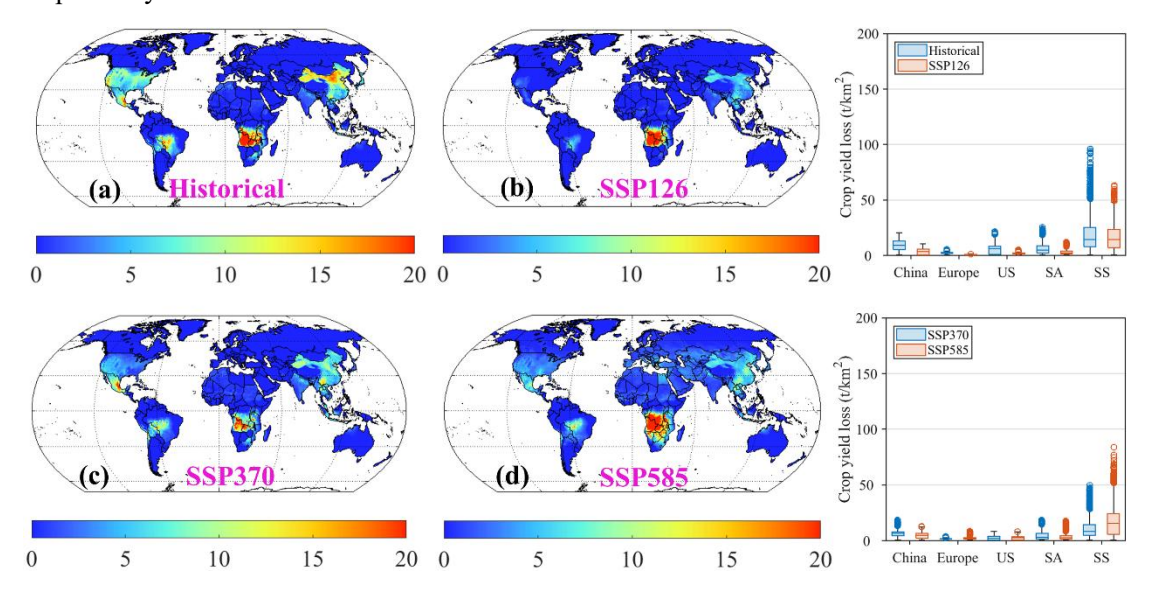


Figure S6 The global variations of wildfire-induced O₃-related spring wheat yield losses (Unit: t/km²) during historical (a), SSP1-2.6 (b), SSP3-7.0 (d), and SSP5-8.5 (e) scenarios during 2040s, respectively. The spatial variations of wildfire-induced spring wheat yield losses (Unit: t/km²) in major regions during 2040s. US, SA, and SS represent the United States, South America, and Sub-Sahara Africa, respectively.

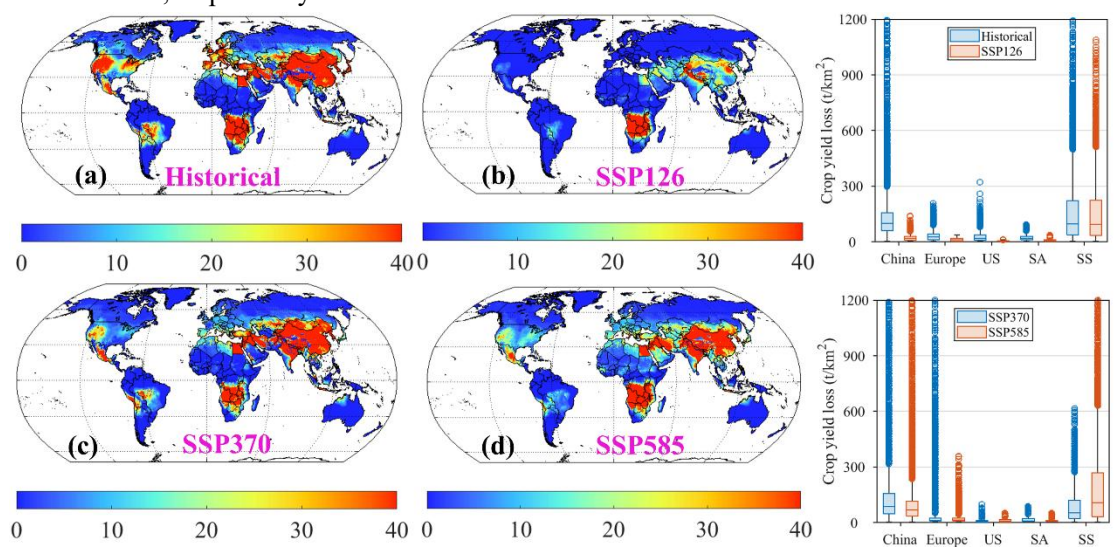


Figure S7 The global variations of wildfire-induced O₃-related winter wheat yield losses (Unit: t/km²) during historical (a), SSP1-2.6 (b), SSP3-7.0 (d), and SSP5-8.5 (e) scenarios during 2040s, respectively. The spatial variations of wildfire-induced winter wheat yield losses (Unit: t/km²) in major regions during 2040s. US, SA, and SS represent the United States, South America, and Sub-Sahara Africa, respectively.

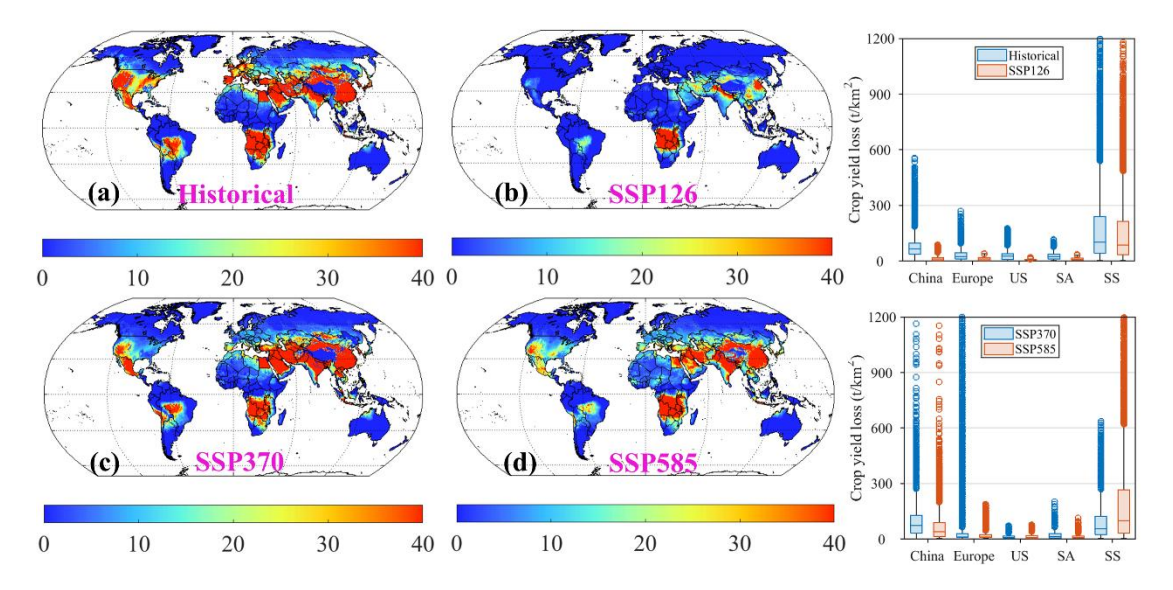


Figure S8 The global variations of wildfire-induced O₃-related maize yield losses (Unit: t/km²) during SSP1-2.6 (a), SSP3-7.0 (b), and SSP5-8.5 (c) scenarios during 2090s, respectively. The global difference of wildfire-induced maize yield losses (Unit: t/km²) in different SSP scenarios during 2090s. US, SA, and SS represent the United States, South America, and Sub-Sahara Africa, respectively.

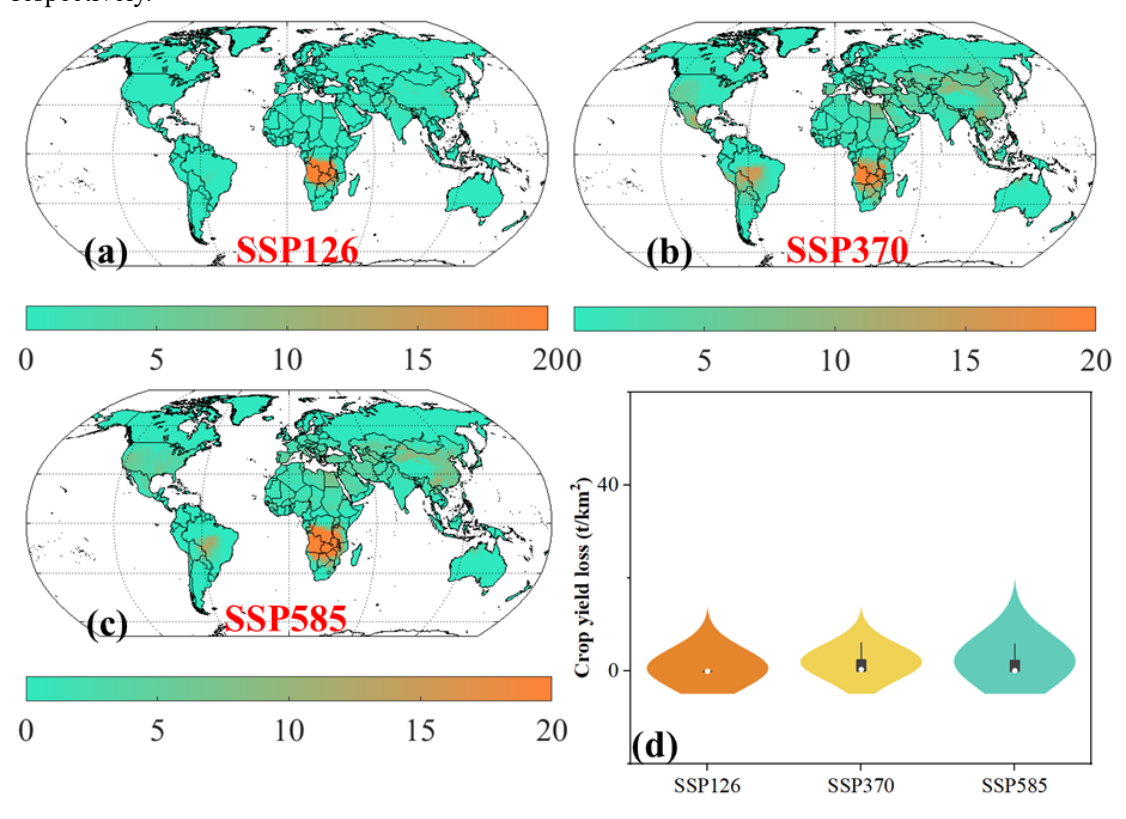


Figure S9 The global variations of wildfire-induced O₃-related rice yield losses (Unit: t/km²) during SSP1-2.6 (a), SSP3-7.0 (b), and SSP5-8.5 (c) scenarios during 2090s, respectively. The global difference of wildfire-induced rice yield losses (Unit: t/km²) in different SSP scenarios during 2090s. US, SA, and SS represent the United States, South America, and Sub-Sahara Africa, respectively.

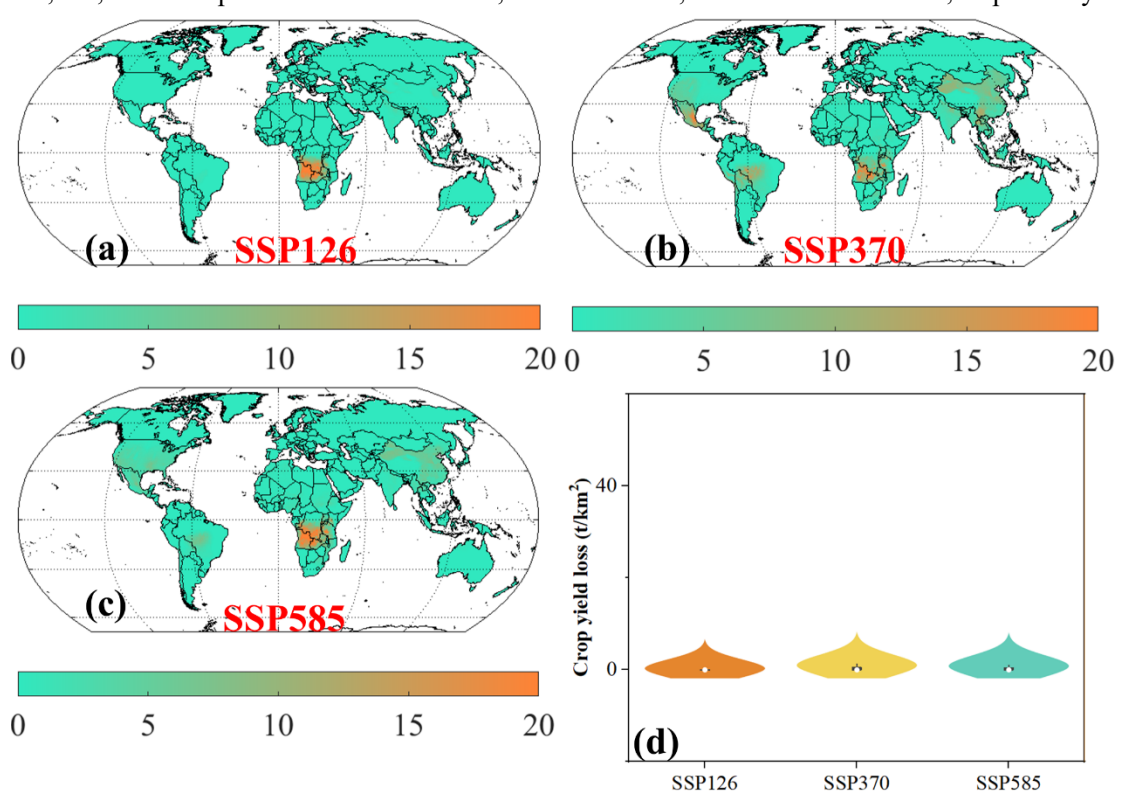


Figure S10 The global variations of wildfire-induced O₃-related spring wheat yield losses (Unit: t/km²) during SSP1-2.6 (a), SSP3-7.0 (b), and SSP5-8.5 (c) scenarios during 2090s, respectively. The global difference of wildfire-induced spring wheat yield losses (Unit: t/km²) in different SSP scenarios during 2090s. US, SA, and SS represent the United States, South America, and Sub-Sahara Africa, respectively.

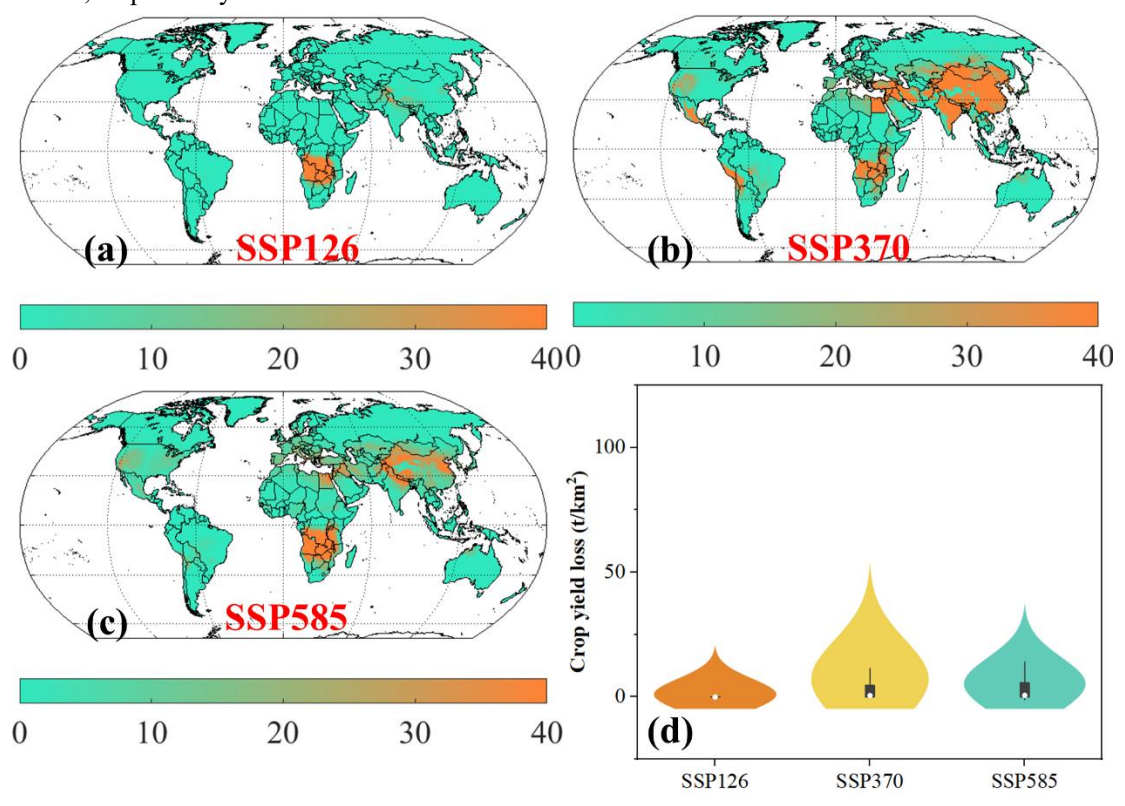
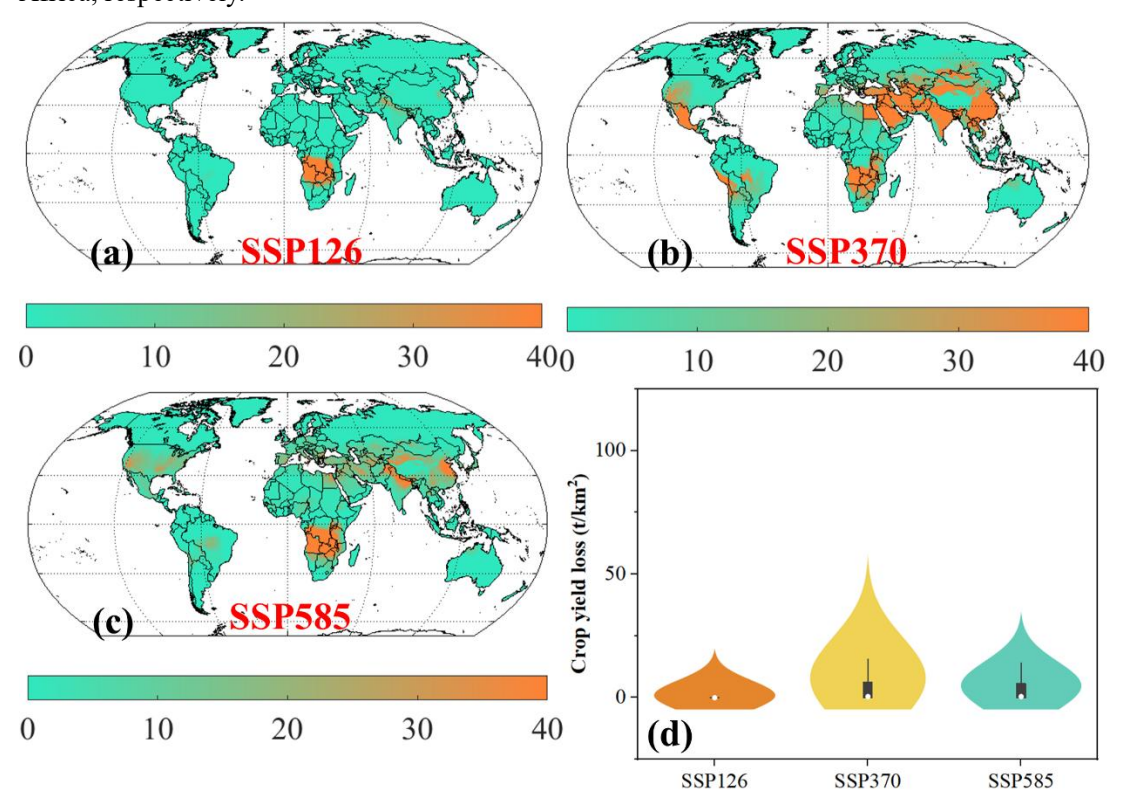


Figure S11 The global variations of wildfire-induced O₃-related winter wheat yield losses (Unit: t/km²) during SSP1-2.6 (a), SSP3-7.0 (b), and SSP5-8.5 (c) scenarios during 2090s, respectively. The global difference of wildfire-induced winter wheat yield losses (Unit: t/km²) in different SSP scenarios during 2090s. US, SA, and SS represent the United States, South America, and Sub-Sahara Africa, respectively.



References

- 1. Peng, J.; Shang, B.; Xu, Y.; Feng, Z.; Pleijel, H.; Calatayud, V., Ozone exposure-and flux-yield response relationships for maize. *Environmental pollution* **2019**, *252*, 1-7.
- 2. Wang, X.; Mauzerall, D. L., Characterizing distributions of surface ozone and its impact on grain production in China, Japan and South Korea: 1990 and 2020. *Atmospheric Environment* **2004**, *38*, (26), 4383-4402.
- 3. Feng, Z.; Kobayashi, K.; Li, P.; Xu, Y.; Tang, H.; Guo, A.; Paoletti, E.; Calatayud, V., Impacts of current ozone pollution on wheat yield in China as estimated with observed ozone, meteorology and day of flowering. *Atmospheric Environment* **2019**, *217*, 116945.